The *Azotobacter vinelandii* NifEN Complex Contains Two Identical [4Fe-4S] Clusters†

Paul J. Goodwin,‡ Jeffrey N. Agar,§ Jon T. Roll,|| Gary P. Roberts,|| Michael K. Johnson,§ and Dennis R. Dean*,‡

Department of Biochemistry, Virginia Polytechnic Institute and State University, Blacksburg, Virginia 24061, Department of Chemistry and Center for Metalloenzyme Studies, University of Georgia, Athens, Georgia 30602, and Department of Bacteriology, University of Wisconsin, Madison, Wisconsin 53706

Received February 24, 1998; Revised Manuscript Received May 21, 1998

ABSTRACT: The nifE and nifN gene products from *Azotobacter vinelandii* form an $\alpha_2\beta_2$ tetramer (NifEN complex) that is required for the biosynthesis of the nitrogenase FeMo cofactor. In the current model for NifEN complex organization and function, the complex is structurally analogous to the nitrogenase MoFe protein and provides an assembly site for a portion of FeMo cofactor biosynthesis. In this work, gene fusion and immobilized metal-affinity chromatography strategies were used to elevate the in vivo production of the NifEN complex and to facilitate its rapid and efficient purification. The NifEN complex produced and purified in this way exhibits an FeMo cofactor biosynthetic activity similar to that previously described for the NifEN complex purified by traditional chromatography methods. UV−visible, EPR, variable-temperature magnetic circular dichroism, and resonance Raman spectroscopies were used to show that the NifEN complex contains two identical $[4Fe\text{-}4S]^{2+}$ clusters. These clusters have a predominantly $S = {}^1/_2$ ground state in the reduced form, exhibit a reduction potential of −350 mV, and are likely to be coordinated entirely by cysteinyl residues on the basis of spectroscopic properties and sequence comparisons. A model is proposed where each NifEN complex [4Fe-4S] cluster is bridged between a NifE−NifN subunit interface at a position analogous to that occupied by the P clusters in the nitrogenase MoFe protein. In contrast to the MoFe protein P clusters, the NifEN complex [4Fe-4S] clusters are proposed to be asymmetrically coordinated to the NifEN complex where NifE cysteines-37, -62, and -124 and NifN cysteine-44 are the coordinating ligands. On the basis of a homology model of the three-dimensional structure of the NifEN complex, the [4Fe-4S] cluster sites are likely to be remote from the proposed FeMo cofactor assembly site and are unlikely to become incorporated into the FeMo cofactor during its assembly.

Biological nitrogen fixation is catalyzed by nitrogenase, a metalloenzyme composed of two-component proteins called the Fe protein and MoFe protein (reviewed in refs *1*−*3*). The Fe protein [also called dinitrogenase reductase (*4*)] is a homodimer that contains a single [4Fe-4S] cluster bridged between its identical subunits (*5*). The MoFe protein (also called dinitrogenase) is an $\alpha_2\beta_2$ tetramer that contains two pairs of novel metalloclusters called the P cluster (Fe_8S_7) and the iron−molybdenum cofactor [FeMo cofactor (Fe_7S_9Mo−homocitrate)]. Each $\alpha\beta$ unit of the MoFe protein is believed to comprise a single catalytic unit that contains one P cluster and one FeMo cofactor that are separated by approximately 17 Å (*6*). During catalysis, the Fe protein delivers electrons to the MoFe protein in a process that involves association and dissociation of the component proteins, MgATP binding, and nucleotide hydrolysis (*4*). The nucleotide binding sites are located on the Fe protein, and a minimum of two MgATP are hydrolyzed for each electron transfer event. The P cluster is located at the $\alpha\beta$ interface of the MoFe protein and appears to function as an intermediate electron carrier site that accepts electrons from the Fe protein and subsequently effects their intramolecular delivery to the FeMo cofactor (*7*−*9*), the site of substrate binding and reduction (*10*−*12*).

Because the FeMo cofactor provides the site of substrate binding and reduction, its structure and assembly have attracted considerable attention. X-ray crystallographic analyses have shown that the FeMo cofactor consists of a metal−sulfur core (Fe_7S_9Mo) and one molecule of (*R*)-homocitrate (*13*). The metal−sulfur core is constructed from Fe_3S_3Mo and Fe_4S_3 fragments that are connected by three inorganic sulfide bridges located between pairs of Fe atoms from opposing fragments. Homocitrate is coordinated to the Mo atom through its 2-hydroxy and 2-carboxyl groups.

Biochemical and genetic studies using both *Azotobacter vinelandii* and *Klebsiella pneumoniae* have revealed that at least six *nif*-specific gene products, including NifB, NifE, NifN, NifV, NifQ, and NifH, are directly involved in the biosynthesis of the FeMo cofactor (*14*). NifB catalyzes the formation of an FeMo cofactor precursor called the B cofactor which is composed of an iron−sulfur core that does

† This work was supported by grants from the National Science Foundation (Grant MCB-9630127 to D.R.D. and Grant MCB-9604446 to G.P.R.) and the National Institutes of Health (Grant GM51962 to M.K.J.) and a National Science Foundation Research Training Group Award (BIR-9413236 to M.K.J.).

* Corresponding author. Telephone: (540) 231-5895. Fax: (540) 231-7126. E-mail: deandr@vt.edu.

‡ Virginia Polytechnic Institute and State University.

§ University of Georgia.

|| University of Wisconsin.

S0006-2960(98)00435-8 CCC: $15.00
Published on Web 06/29/1998

not include Mo or homocitrate (*15*). NifE and NifN form an $\alpha_2\beta_2$ tetramer (*16*) that is able to bind the B cofactor (*17*, *18*), and in doing so provide a scaffold for one or more steps in FeMo cofactor biosynthesis. NifQ appears to have a role in the activation of Mo for FeMo cofactor assembly (*19*), and NifV is a homocitrate synthase that provides the organic constituent of the FeMo cofactor (*20*, *21*). The role of NifH (Fe protein) in FeMo cofactor assembly is not yet understood, but its role does not appear to involve either electron transfer or MgATP hydrolysis (*22*−*24*). The Fe protein and the product of another gene [NifY in the case of *K. pneumoniae* (*25*, *26*) and a protein called γ in the case of *A. vinelandii* (*27*, *28*)] also appear to have some role in the incorporation of the FeMo cofactor into the apo-MoFe protein.

Most of what is known about the assembly of the FeMo cofactor has involved the application of in vitro reconstitution (*10*) and in vitro biosynthetic assays (*29*) developed by Shah and co-workers. For example, in vitro reconstitution assays were used to show that the FeMo cofactor is separately synthesized and then inserted into the apo-MoFe protein rather than being assembled stepwise into the apo-MoFe protein (*30*). This observation, primary sequence comparisons (*31*, *32*), and the two-dimensional electrophoretic properties of NifE and NifN ultimately led to the hypothesis that the NifEN complex provides a molecular scaffold for at least a portion of FeMo cofactor biosynthesis (*31*). In related experiments, it was found that NifB- and NifE- or NifN-deficient extracts could be mixed to achieve FeMo cofactor formation, providing that Mo and MgATP were also added to the reaction mixture (*29*). Experiments of this sort provided an assay that permitted the isolation of small amounts of the NifEN complex (*16*), which was shown to be an $\alpha_2\beta_2$ tetramer that contains Fe−S cluster(s). One problem encountered in the isolation and characterization of FeMo cofactor biosynthetic enzymes is that they are only present in very low intracellular amounts. To date, this feature has precluded the purification of the NifEN complex in the quantities necessary for detailed biophysical characterization of its associated Fe−S cluster(s). In this work, a gene fusion approach for overproduction of the NifEN complex in *A. vinelandii* and the application of immobilized metal-affinity chromatography for NifEN complex purification are described. These procedures have permitted purification of the active NifEN complex in sufficient quantities for biophysical characterization.

EXPERIMENTAL PROCEDURES

DNA Biochemistry and Strain Constructions. Transformation of *A. vinelandii* was performed as previously described by Page and von Tigerstrom (*33*). Strain DJ1061 (Figure 1) was constructed in several steps. In the first step, polymerase chain reaction (PCR)-directed DNA amplification and mutagenesis were used to obtain an approximately 0.9 kb *Msc*I−*Sal*I fragment of *A. vinelandii* genomic DNA (*31*) that was incorporated into *Sma*I−*Sal*I-digested pUC119 vector DNA. This plasmid was designated pDB902, and it contains the *A. vinelandii nifE* promoter, as well as upstream and downstream sequences extending approximately 450 base pairs in each direction. Plasmid pDB902 was also constructed so that a unique *Nde*I restriction enzyme site overlaps the *nifE* translation initiation site. Plasmid pDB904 was constructed by digesting pDB902 with *Nde*I and

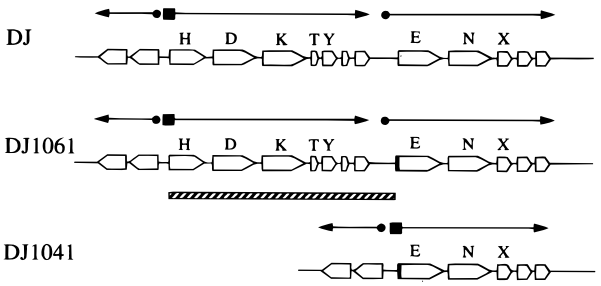

FIGURE 1: Organization of nif-specific genes in various strains relevent to this work. Horizontal arrows indicate the direction of transcription. The approximate position of the nifH promoter is indicated by a filled box, and filled circles indicate the approximate positions of promoters for other transcription units. The crosshatched bar indicates the region deleted from the chromosome in construction of DJ1041. The filled portion at the begininng of the nifE gene for DJ1061 and DJ1041 indicates the position of the sequence encoding the respective polyhistidine tags.

incorporating a kanamycin-resistance cartridge derived from pUC4-KAPA (*34*) at the *Nde*I site of pDB902. Plasmid pDB906 was constructed by digesting pDB902 with *Nde*I and then ligating a synthetic DNA cartridge into this site. The sense strand of the synthetic cartridge has the sequence 5′TATGCATCACCACCATCACCACCA3′. The triplet that corresponds to the *nifE* translation initiation codon is underlined in the synthetic DNA cartridge shown above. This construction places seven in-frame histidine codons between the initiating methionine codon and the second codon of the cloned portion of *nifE* carried on pDB906. Restriction enzyme mapping and DNA sequence analyses were used to confirm all plasmid constructions. Wild-type *A. vinelandii* cells were transformed using pDB904 DNA as the donor and then selecting for kanamycin resistance and scoring for ampicillin sensitivity. One transformant that resulted from double-reciprocal crossover events, and which is Nif-minus, kanamycin^R, and ampicillin^S, was designated DJ1057. Strain DJ1061 was constructed by transformation of DJ1057, using pDB906 DNA as the donor, resulting in a Nif-plus, kanamycin^S phenotype. Strain DJ1061 is genotypically identical to the wild type except that there are seven histidine codons immediately following the initiating methionine codon at the N terminus of *nifE*. It should be noted that none of the plasmids used for strain constructions described in this work are capable of autonomous replication in *A. vinelandii*.

Strain DJ1041 (Figure 1) was also constructed in several steps. In the first step, a DNA cartridge, extending from the *nifH* translation initiation site to approximately 500 base pairs upstream, was generated by PCR amplification. This cartridge was constructed so that an *Nde*I restriction enzyme site was located at the *nifH* translation initiation site, and a *Bgl*II site was located approximately 500 base pairs upstream of the *nifH* translation initiation site. This cartridge was digested by *Nde*I and *Bgl*II and ligated into *Nde*I−*Bgl*II-digested pT$_7$-7 plasmid vector DNA (*35*) to form plasmid pDB591. In the second step, a *nifE* gene cartridge was generated by PCR amplification so that an *Nde*I site was located at the *nifE* initiation codon and a *Bam*HI site was located shortly downstream of the *nifE* coding sequence. This cartridge was ligated into *Nde*I−*Bam*HI-digested pT$_7$-7 vector DNA to form pDB558. In the next step, pDB558 was digested with *Nde*I and *Bam*HI and the resulting *nifE* cartridge purified and ligated into *Nde*I−*Bam*HI-digested

pDB591 to form pDB597. Construction of pDB597 results in a fusion of the *nifH* transcriptional and translational elements to the coding portion of the *nifE* gene. In the final step of plasmid construction, pDB597 was digested with *Nde*I and ligated with the same synthetic DNA cartridge described above, forming plasmid pDB867. This construction places seven in-frame histidine codons between the initiating methionine codon and the second codon of the *nifE* coding sequence. The fusion of the *nifH* promoter sequence with the *nifE* coding sequence carried by pDB867 was then transferred to the *A. vinelandii* chromosome to yield strain DJ1041. This construction was accomplished by transformation using congression (coincident transfer of unlinked genetic markers) where the rifampicin-resistance marker contained in pDB303 (*36*) was used as the selected marker. The phenotype of DJ1041 is Nif^- and Rif^R.

Cell Growth, Purification of the NifEN Complex, and Assays. A. vinelandii cells were grown at 30 °C in a 150 L custom-built fermenter (W. B. Moore, Inc., Easton, PA) in modified Burk medium (*37*) containing 10 μM Na_2MoO_4 and 10 mM urea. Cultures were sparged with pressurized air (80 L/min at 5 psi) and agitated at 125 rpm. When the cell density reached 180 Klett units (red filter), they were derepressed for *nif* expression by concentration and resuspension in Burk medium with no added nitrogen source (*38*). Harvested cells were stored at −80 °C until they were used. Crude extracts were prepared by the osmotic shock method (*39*) in degassed buffer containing 25 mM Tris-HCl (pH 7.9) and 1 mM sodium dithionite. Prior to NifEN complex purification, the extracts were made 500 mM in NaCl by the addition of degassed, granular NaCl. All biochemical manipulations were performed under an argon atmosphere using a Schlenk apparatus. Approximately 120 g of cells (wet weight) was processed for each purification, yielding approximately 10 g of total protein in the crude extract. The NifEN complex was purified using immobilized metal-affinity chromatography (IMAC) and DEAE-sepharose anion-exchange chromatography (Amersham-Pharmacia, Piscataway, NJ). Cell extracts were loaded on an IMAC Zn(II)-charged column (30 mL of resin in a 1.5 cm × 15 cm column) using a peristaltic pump. After the extract was loaded, the column was washed with 3 column volumes of the above buffer containing 20 mM imidazole hydrochloride. The protein that remained bound to the column was then eluted using the above buffer containing 250 mM imidazole hydrochloride. The eluted protein was collected and diluted 7-fold in a degassed buffer (25 mM Tris-HCl at pH 7.9) containing 1 mM sodium dithionite. The diluted protein was then loaded onto a DEAE-sepharose column (30 mL of resin in a 1.5 cm × 15 cm column) and eluted using a linear NaCl gradient (100 to 300 mM NaCl over 5 column volumes). The NifEN fraction, which eluted at approximately 250 mM NaCl, was collected and concentrated using an Amicon concentrator (Beverly, MA) fitted with a YM100 filter. Concentrated protein was pelleted and stored in liquid nitrogen until it was used. Protein purity was monitored by SDS−PAGE as previously described (*38*). Protein was quantitated by the BCA method using bovine serum albumin as the standard (*40*).

NifEN activity was determined by slight modifications of previously described procedures (*16*, *18*). Each degassed 9 mL reaction vial included 0−60 μg of isolated NifEN, 100 μL of 25 mM Tris-HCl (pH 7.4, 1.0 mM sodium dithionite), 20 μL of 5 mM homocitrate, 10 μL of 1.0 mM Na_2MoO_4, 200 μL of an ATP-regenerating system (containing 3.6 mM ATP, 6.3 mM $MgCl_2$, 51 mM phosphocreatine, 20 units/mL creatine phosphokinase, and 6.3 mM sodium dithionite), and 200 μL of DJ1007 (Δ*nifE*) crude extract. The reaction vial also included an excess of the B cofactor, which is necessary for FeMo cofactor biosynthesis [20 μL of an isolated B cofactor preparation (60 mg of Fe/L) provided by V. K. Shah was used (*15*)]. Vials were incubated at 30 °C for 30 min to allow FeMo cofactor biosynthesis and insertion into the apo-MoFe protein present in the DJ1007 crude extract. An additional 800 μL of the ATP-regenerating system was then added; the vials were brought to 1 atm, and a 30 min acetylene reduction assay was performed under a 10% acetylene atmosphere at 30 °C. Ethylene formation was monitored using a Hewlett-Packard 5890A gas chromatograph equipped with a FID detector. The amount of apo-MoFe protein present in the DJ1007 extract was estimated by the reconstitution system using the isolated FeMo cofactor (100 mg of Fe/L) as previously described (*10*). The FeMo cofactor used in this work was a gift from V. K. Shah.

Metal Analysis. Fe was quantitated by the α,α'-bipyridyl method (*41*), and Mo was quantitated by inductively coupled plasma emission (Utah State University's Soil Testing Laboratory, Logan, UT).

Preparation of Antisera against NifN. For the preparation of antibodies against NifN for use in Western analyses, NifN was produced at a high level in *Escherichia coli* and purified. For this purpose, a PCR-generated *nifN* gene cartridge was cloned into the *Nde*I−*Bam*HI sites of the cloning vector pT_7-7 to form pDB560. This construct places expression of *nifN* under control of the T_7 control elements. Plasmid pDB560 was then transformed into the *E. coli* host strain BL21(DE3). NifN was then produced at a high level and purified by using essentially the same procedures previously described for the high level of expression and purification of NifU (*42*). Purified NifN was then sent to Cocalico Biologicals Inc. (Reamstown, PA) for commercial production of rabbit anti-NifN antisera. Chemicals for Western analysis were obtained from ICN Biomedicals (Costa Mesa, CA), and the procedures recommended by the supplier were followed.

Spectroscopic Characterization of NifEN. The sample concentrations given in the figure captions are based on the quantitation of the purified protein solution by the BCA method (*40*). Spectroscopic results were quantified per $\alpha\beta$ heterodimer. UV−visible absorption spectra were recorded under anaerobic conditions in septum-sealed 1 mm cuvettes using a Shimadzu 3101PC scanning spectrophotometer. Variable-temperature magnetic circular dichroism (VTMCD)[1] spectra were recorded on samples containing 55% (v/v) glycerol in 1 mm cuvettes using an Oxford Instruments Spectromag 4000 (0−7 T) split coil superconducting magnet (1.5−300 K) mated to a Jasco J-715C spectropolarimeter. Experimental protocols used for VTMCD studies were performed as previously described (*43*, *44*). X-Band (~9.6 GHz) electron paramagnetic resonance (EPR) spectra were recorded on a Bruker ESP-300E EPR spectrometer equipped

[1] Abbreviations: VTMCD, variable-temperature magnetic circular dichroism; RR, resonance Raman; NHE, normal hydrogen electrode.

with a dual-mode ER-4116 cavity and an Oxford Instruments ESR-9 flow cryostat. Frequencies were measured with a Systron-Donner 6054B frequency counter, while the magnetic field was calibrated with a Bruker ER035M gaussmeter. Spin quantitations were carried out under nonsaturating conditions with 1 mM Cu(II)EDTA as the standard, using the procedures outlined by Aasa and Vänngård (*45*).

Resonance Raman spectra were recorded using an Instruments SA Ramanor U1000 spectrometer fitted with a cooled RCA 31034 photomultiplier tube with 90° scattering geometry. Spectra were recorded digitally using photon-counting electronics, and signal:noise was improved by signal averaging of multiple scans. Band positions were calibrated using the excitation frequency and CCl_4 and are accurate to ± 1 cm^{-1}. Laser excitation lines were from a Coherent Innova 100 10 W argon ion laser, with plasma lines removed using a Pellin Broca Prism premonochromator. Resonance Raman samples were placed in a specially designed sample cell (*46*) at the end of an Air Products Displex model CSA-202E closed-cycle refrigerator and remained at 28 K under an atmosphere of argon throughout scanning. The low sample temperature facilitates improved spectral resolution and prevents laser-induced sample degradation. Scattering was collected from the surface of a frozen 12 μL droplet.

EPR redox titration was performed at ambient temperature (25−27 °C) in a glovebox under anaerobic conditions, using 20 mM Tris-HCl buffer (pH 7.9) and 300 mM NaCl. The concentration of the NifEN complex was 140 μM. Each mediator dye was added to a concentration of 50 μM to cover the range of −500 to −100 mV (vs NHE). The mediator dyes used were methyl viologen, benzyl viologen, neutral red, safranin O, anthraquinone-2-sulfonate, phenosafranin, and anthraquinone-1−5-disulfonate. Samples were first reduced by addition of excess sodium dithionite followed by oxidative titration with potassium ferricyanide. Potentials were measured with a platinum working electrode and a saturated Ag/AgCl reference electrode. After equilibration at the desired potential, a 250 μL aliquot was transferred to a calibrated EPR tube and frozen immediately in liquid nitrogen. Redox potentials are reported relative to the NHE.

RESULTS

Expression and Purification of the NifEN Complex. Figure 1 shows a schematic of the relevant genomic *nif* region for the wild type (DJ) and the two strains (DJ1061 and DJ1041) that were constructed by gene-directed mutagenesis and gene-replacement techniques. Strain DJ1041 was designed for (a) the elevated production of the *nifEN* gene products and (b) the facile purification of the NifEN complex using IMAC. The first of these goals was achieved by deleting the intervening region between the relatively strong *nifH* promoter and the *nifEN* structural genes, thereby placing the expression of *nifEN* under the direction of the *nifH* transcriptional and translational control elements. The second goal was made possible by placing seven histidine codons between the methionine initiation codon and the second codon of the *nifE* coding sequence. Strain DJ1061 was constructed to (a) determine whether insertion of the polyhistidine coding sequence at the N terminus of *nifE* alters the in vivo activity of the NifEN complex and (b) permit the comparison of the relative amounts of the NifEN complex

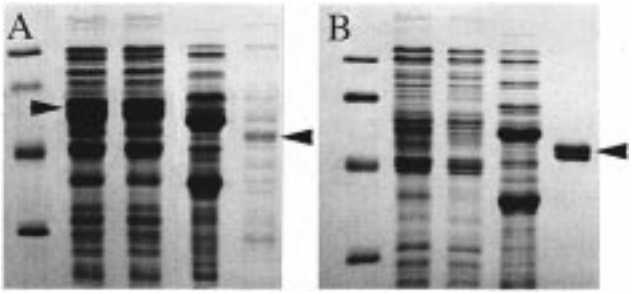

FIGURE 2: IMAC purification of the NifEN complex from DJ1061 (A) and DJ1041 (B). The proteins were separated by 12% SDS−PAGE and stained with Coomassie brilliant blue: lane 1, M_r standards (phosphorylase *b*, bovine serum albumin, carbonic anhydrase, and soybean trypsin inhibitor); lane 2, crude extract; lane 3, column flow through; lane 4, 20 mM imidazole hydrochloride wash fraction; and lane 5, purified NifEN complex. Arrows pointing left indicate the position of NifE (upper band) and NifN (lower band). The arrow pointing right in panel A indicates the position of the MoFe protein α- and β-subunits. Corresponding MoFe protein subunit bands are not seen in panel B because *nifDK* genes have been deleted in strain DJ1041.

that accumulate when *nifEN* expression is driven by either the *nifE* or *nifH* control elements. Both the wild type and DJ1061 grow at the same rate (doubling time of 2.2−2.4 h) when cultured under diazotrophic growth conditions. Thus, because strains without *nifE* are unable to grow diazotrophically (*32*), this result indicates that placement of the polyhistidine tail at the N-terminal region of NifE does not impair the NifEN complex to an extent that can be detected in vivo.

Panels A and B of Figure 2 show SDS−PAGE profiles for fractions obtained during the purification of the NifEN complex from DJ1061 and DJ1041, respectively. The simple four-step purification procedure involves (i) passing a crude extract prepared from *nif*-derepressed cells over a Zn(II)-charged IMAC column, (ii) washing the column with a 20 mM imidazole hydrochloride buffer, (iii) eluting the bound protein with 250 mM imidazole hydrochloride buffer, and (iv) anion-exchange column chromatography. The relative amounts of the NifEN complex purified from DJ1061 and DJ1041 shown in Figure 2, which represent different purifications performed on different days, cannot be quantitatively compared. Nevertheless, examination of the individual panels in Figure 2, which compare individual fractions at different stages of purification, clearly indicates that the amount of the NifEN complex that can be purified from DJ1041 is much higher than that from DJ1061. About 70 mg of the pure NifEN complex can be routinely obtained from 10 g of the DJ1041 crude extract protein, whereas only about 7 mg of the NifEN complex can be obtained from the same amount of the DJ1061 crude extract protein. Also, the estimated amount of the NifEN complex obtained from DJ1061 crude extracts is probably an overestimation because there is a significant amount of contaminating proteins in the purified sample from DJ1061, as can be seen by inspection of lane 5 in Figure 2A. Identification of the protein bands marked as NifEN in Figure 2 was confirmed in two different ways. First, bands at a similar location were not recognized when the crude extract from the wild-type strain was processed in the same way. This result is consistent with the fact that NifE from the parental wild-type strain does not have a polyhistidine tail. Second, the

bands corresponding to NifN in Figure 2 were identified by Western analysis (data not shown) using rabbit antibodies raised against the purified NifN protein that was heterologously expressed in *E. coli*. Although the amount of the NifEN complex accumulated by DJ1041 is much greater than that accumulated by DJ1061, the yield is still lower than might be expected for proteins whose synthesis is directed by the *nifH* control elements. For example, in related studies, we have also placed a polyhistidine tag near the N terminus of *nifD*, which encodes the α-subunit of the MoFe protein, and whose synthesis is naturally directed by the *nifH* promoter. By using the same IMAC approach described here for NifEN purification, 350 mg of the polyhistidine-tagged MoFe protein, having full catalytic activity (≈2000 nmol of H_2 evolved min^{-1} mg^{-1} of protein), can be routinely isolated from 10 g of the nitrogenase-derepressed crude extract (J. Christiansen, P. J. Goodwin, L. Zheng, and D. R. Dean, unpublished). Although it is not known why NifEN from DJ1041 accumulates at levels lower than might be expected, it was found that the amount of NifEN that can be detected in crude extracts by Western analysis drops dramatically after about 3 h of nitrogenase derepression (data not shown). This result indicates that the NifEN complex might have a relatively short in vivo half-life. Roll et al. (*18*) have also reported that the yield of the NifEN complex obtained by using other purification methods is dependent upon the genetic background from which the complex is isolated.

IMAC-Purified NifEN Complex Activity. Previous work has shown that the NifEN complex isolated from a *nifB*-deficient *A. vinelandii* strain can be added to a *nifEN*-deficient crude extract to achieve activation of the apo-MoFe protein, providing other factors necessary for FeMo cofactor biosynthesis (MgATP, Mo, and homocitrate) are also included (*16*, *18*). Furthermore, FeMo cofactor biosynthetic activity is maximized in this system when an excess of the B cofactor, the product of NifB activity, is also added to the reaction mixture. In this work, it was important to establish that the NifEN complex isolated by the IMAC method has the same composition as and an ability to participate in FeMo cofactor biosynthesis similar to that previously reported for the NifEN complex isolated by other methods. These features were demonstrated in the following ways. The ability of IMAC-purified NifEN complex to activate the apo-MoFe protein in extracts prepared from a *nifE*-deletion mutant was shown to be almost identical to that described for the NifEN complex that was purified using the original purification scheme reported by Paustian et al. (Figure 3B; see Figure 5 in ref *16*). The maximum amount of activation of the apo-MoFe protein effected by the IMAC-purified NifEN complex (Figure 3B) also corresponds to the maximum amount of reconstitution that can be achieved by addition of the isolated FeMo cofactor to the same extract (Figure 3A). The IMAC-purified NifEN complex was shown to be an $\alpha_2\beta_2$ tetramer by its mobility on a gel exclusion chromotography column (data not shown). It was also found that, like the NifEN complex previously characterized (*16*), IMAC-purified NifEN is oxygen-labile, contains Fe, and exhibits a characteristic UV−visible spectrum in its oxidized and reduced states (Figure 4).

Biophysical Characterization of the NifEN Complex Fe−S Clusters. (1) UV−Visible Absorption. Figure 4 shows the UV−visible absorption of oxidized and reduced NifEN. The

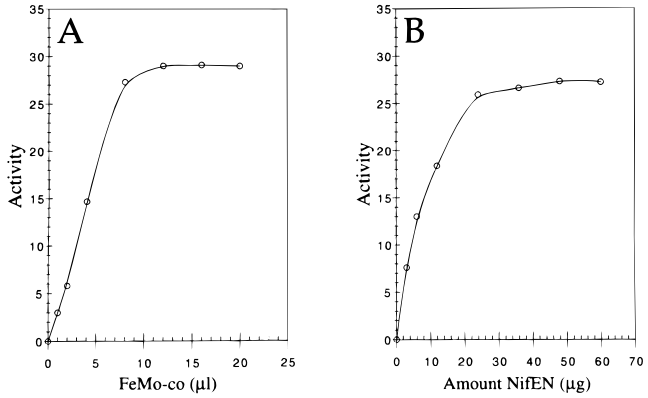

FIGURE 3: Reconstitution of the apo-MoFe protein using either the isolated FeMo cofactor (A) or the FeMo cofactor biosynthesis system (B), as described in Experimental Procedures. MoFe protein activity is expressed as nanomoles of ethylene produced per minute. Assay conditions are described in Experimental Procedures. For the biosynthetic assay shown in panel B, all known components required for FeMo cofactor biosynthesis are present in excess except for the NifEN complex. The same crude extract (9.0 mg for each assay) was used for all reconstitution assays shown in panels A and B. Data points represent the average of two independent assays.

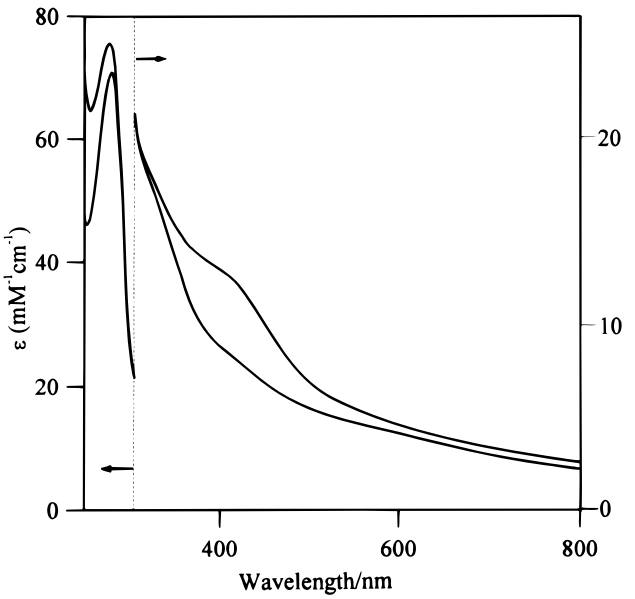

FIGURE 4: UV−visible absorption for oxidized and reduced NifEN. Excess sodium dithionite was removed from reduced NifEN (lower spectrum) by anaerobic buffer exchange. NifEN was oxidized with thionine (upper spectrum), and the excess was removed by anaerobic buffer exchange.

oxidized spectrum with its pronounced shoulder at 410 nm is characteristic of proteins containing $[4Fe\text{-}4S]^{2+}$ clusters (*47*). Upon reduction with dithionite, the peak at 410 nm is diminished and a broad featureless spectrum indicative of a $[4Fe\text{-}4S]^{+}$ cluster appears. The molar extinction coefficients for oxidized (ϵ_{410} = 13 500 M^{-1} cm^{-1}) and reduced (ϵ_{390} = 9500 M^{-1} cm^{-1}) NifEN (expressed per $\alpha\beta$ dimer) indicate two $[4Fe\text{-}4S]^{2+}$ clusters per NifEN $\alpha_2\beta_2$ tetramer. These results are also consistent with iron analyses of NifEN, which indicate 9.5 ± 0.5 iron atoms per $\alpha_2\beta_2$ tetramer, with no Mo detected.

(2) EPR and EPR-Monitored Redox Titration. X-Band EPR spectra of dithionite-reduced NifEN were recorded at temperatures in the range of 4.2−100 K with microwave powers between 0.001 and 100 mW. A less extensive series

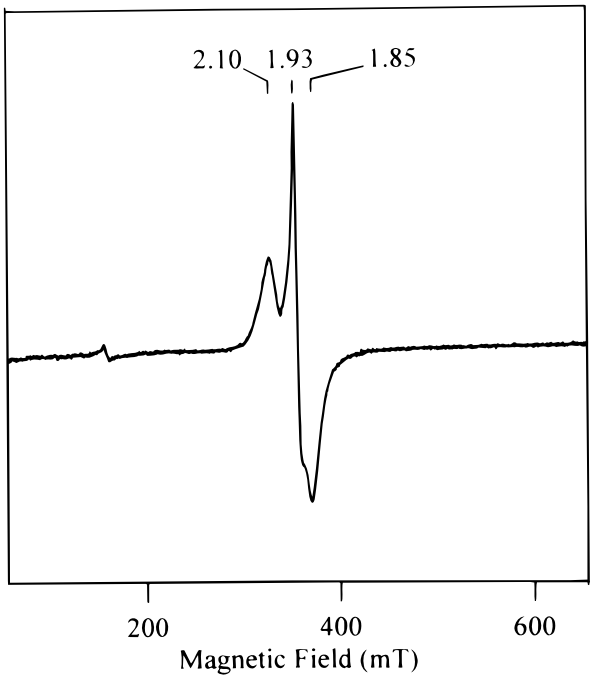

FIGURE 5: X-Band EPR spectrum of dithionite-reduced NifEN. The sample (0.4 mM) was in 20 mM Tris-HCl buffer (pH 7.9) with 1 mM sodium dithionite. Conditions of measurement: microwave frequency, 9.6 GHz; modulation amplitude, 0.64 mT; microwave power, 20 mW; and temperature 10 K.

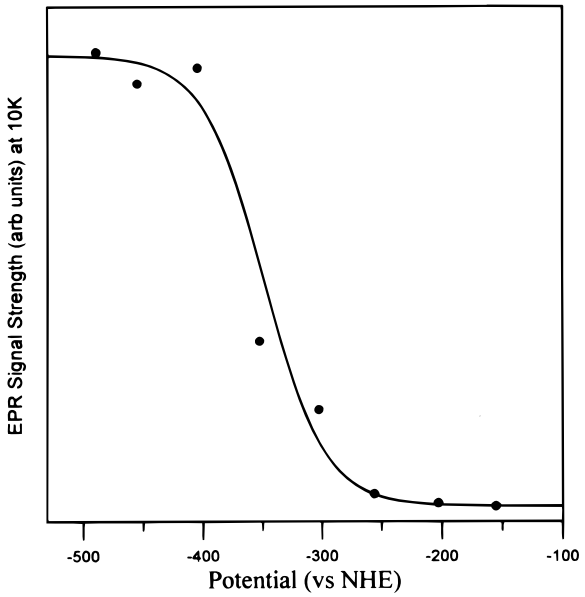

FIGURE 6: EPR signal intensity (arbitrary units) for NifEN (0.15 mM) as a function of poised potential. Dye-mediated redox titrations were carried out as described in Experimental Procedures. Data points correspond to the peak-to-trough intensity ($g = 1.93-1.85$) at 10 K. The solid line represents a one-electron Nernst equation with a midpoint potential (vs NHE) of −350 mV. EPR conditions: temperature, 10 K; microwave power, 20 mW; modulation amplitude, 1.02 mT; and microwave frequency, 9.60 GHz.

of experiments were conducted on NifEN samples containing 55% (v/v) glycerol (i.e., the same samples used for VTMCD studies), and the EPR properties were found to be unperturbed by the presence of glycerol. A representative EPR spectrum of dithionite-reduced NifEN is shown in Figure 5. The protein exhibits a rhombic spectrum ($g = 2.10$, 1.92, and 1.85) that is only discernible at temperatures below 30 K. This resonance accounts for 1.1 spins per $\alpha\beta$ dimer, and except for a minor adventitious Fe^{3+} ion signal centered at $g = 4.3$, there was no evidence of any $S > {}^1/_2$ resonances in the low-field region. Taken together, the spin quantitation, g values, and relaxation properties indicate there are two $S = {}^1/_2$ $[4Fe\text{-}4S]^+$ clusters per $\alpha_2\beta_2$ tetramer. To assess the midpoint potential of the $[4Fe\text{-}4S]^{2+}$ couple, a dye-mediated EPR-monitored redox titration of purified NifEN was carried out at pH 7.9. Figure 6 shows a plot of the intensity of the $S = {}^1/_2$ resonance as a function of potential. A one-electron Nernst plot overlays the individual data points to a good approximation, indicating a midpoint potential of -350 ± 20 mV.

(3) VTMCD. Temperature-dependent MCD bands are observed throughout the 300−800 nm region in the VTMCD spectra of reduced NIFEN (Figure 7). The pattern of these bands is characteristic of a $[4Fe\text{-}4S]^+$ cluster (*47*−*50*), with the derivative feature centered around 410 nm arising at least in part from a very minor heme contaminant. While the absence of a pronounced negative feature centered around 650 nm is generally indicative of an $S = {}^3/_2$ $[4Fe\text{-}4S]^+$ cluster (*48*, *49*), MCD magnetization data collected at 536 nm (Figure 9) indicate that the cluster ground state is predominantly $S = {}^1/_2$, in accord with the EPR results. The magnetization data collected at three fixed temperatures (1.8, 4.2, and 10.0 K) are fit to first approximation by theoretical data constructed using the EPR-determined g values ($g_{||} =$ 2.10 and $g_\perp = 1.89$). The intensities of the low-temperature MCD spectra of paramagnetic Fe−S clusters, compared under equivalent conditions after normalizing for concentration and path length, and correcting for sample depolarization (*43*, *44*), provide an approximate estimation of cluster concentration. Synthetic and biological $S = {}^1/_2$ $[4Fe\text{-}4S]^+$ clusters have $\Delta\epsilon$ values for the positive band at 520 nm in the range of 60−90 M^{-1} cm^{-1} at 4.5 T and 2 K (*47*, *48*). The 2 K MCD spectrum of NifEN, which has a $\Delta\epsilon$ of 76

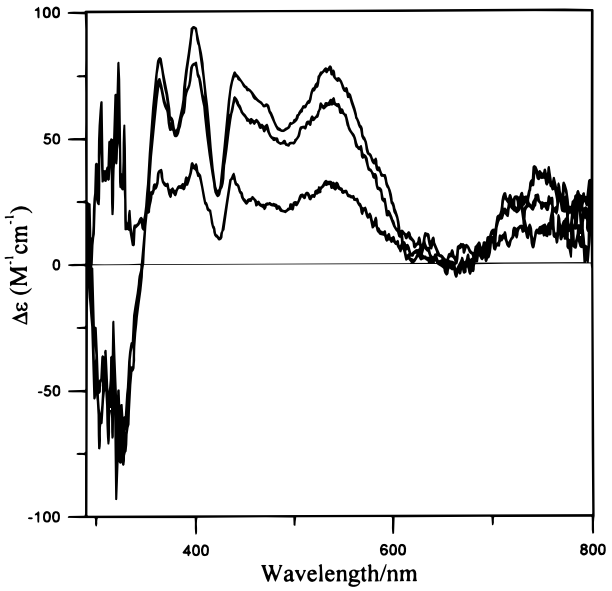

FIGURE 7: VTMCD spectra of dithionite-reduced NifEN. The sample (0.1 mM) was in 20 mM Tris-HCl buffer (pH 7.9) with 1 mM sodium dithionite and 55% (v/v) glycerol. The MCD spectra were recorded in a 1 mm cuvette with a magnetic field of 6.0 T, at 1.8, 4.2, and 10.0 K. All bands increase in intensity with decreasing temperature.

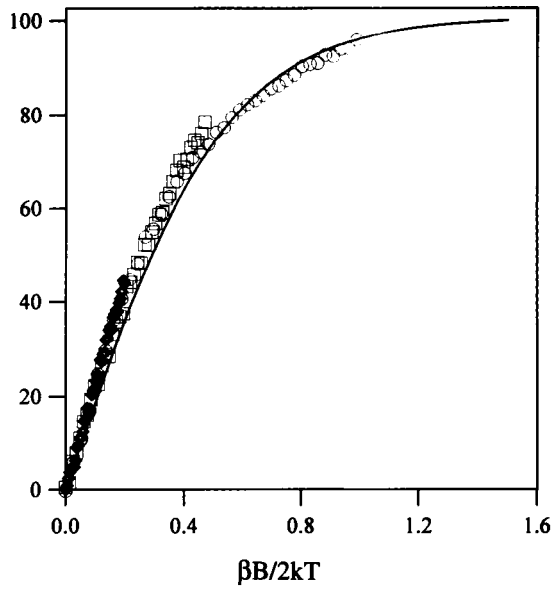

FIGURE 8: MCD magnetization data for dithionite-reduced NifEN. The sample is described in Figure 7. NifEN magnetization data collected at 536 nm using magnetic fields between 0 and 6 T and fixed temperatures: 10.0 (◇), 4.2 (□), and 1.8 K (○). The solid line depicts theoretical magnetization data for an $S = {}^1/_2$ ground state using EPR-determined g values ($g_{||} = 2.10$ and $g_{\perp} = 1.89$) and with an $m_{z/xy}$ of 1.1.

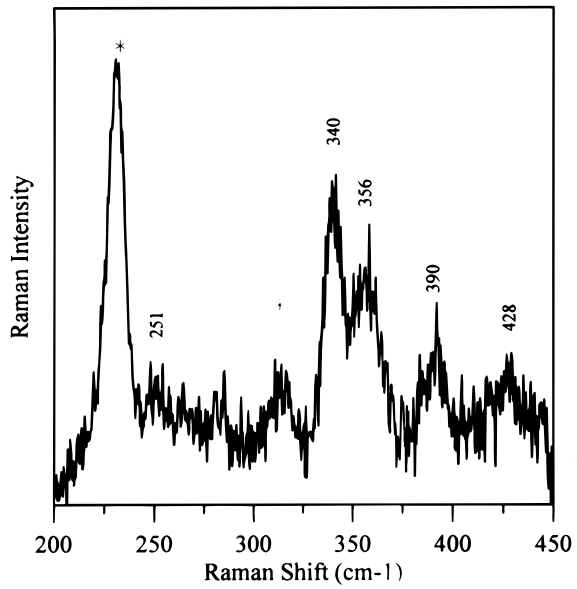

FIGURE 9: Low-temperature resonance Raman spectra of thoinin-oxidized NifEN. The protein concentration was ~3 mM, and the buffering medium was 20 mM Tris-HCl (pH 7.9). The spectrum was obtained at 28 K using 457.9 nm argon laser excitation and is the sum of 103 scans. Each scan involved advancing the spectrometer in 0.5 cm^{-1} increments, and photon counting for 1 s/point with 6 cm^{-1} spectral resolution. A linear ramp was subtracted to correct for background fluorescence, and lattice modes of ice are indicated by an asterisk.

M^{-1} cm^{-1} when quantified per $\alpha\beta$ heterodimer, complements the UV−visible molar extinction coefficients and the EPR spin quantitation in suggesting that there is one [4Fe-4S]$^+$ cluster per NifEN $\alpha\beta$ heterodimer.

(4) Resonance Raman. Resonance Raman spectra in the Fe−S stretching region (200−450 cm^{-1}) provide a means of identifying both Fe−S types in diamagnetic redox states (*51*, *52*) and assessing the cluster ligation (*49*, *53*). The RR spectrum of the thionine-oxidized NifEN complex obtained with 457.9 nm laser excitation is shown in Figure 9. The vibrational frequencies and relative intensities of the Fe−S stretching modes are characteristic of those established for [4Fe-4S]$^{2+}$ clusters (*54*, *55*) and can be assigned by direct analogy under idealized tetrahedral symmetry for the $Fe_4S_4{}^bS_4{}^t$ unit (b = bridging and t = terminal), i.e., (T_2) Fe−S^b, 251 cm^{-1}; (T_1) Fe−S^b, 265 cm^{-1}; (E) Fe−S^b, 280 cm^{-1}; (A_1) Fe−S^b, 340 cm^{-1}; (T_2) Fe−S^t, 356 cm^{-1}; (T_2) Fe−S^b, 383 cm^{-1}; and (A_1) Fe−S^t, 390 cm^{-1}. For example, resonance Raman spectra having similar relative band intensities and frequencies are observed for the [4Fe-4S]$^{2+}$ cluster contained in the nitrogenase Fe protein (*56*) and in synthetic analogue complexes having benzyl thiolate ligands (*54*). The frequency of the most intense band, which corresponds to the totally symmetric breathing mode of the Fe_4S_4 cubane, has been found to a be a useful indicator of noncysteinyl coordination at a specific Fe (*49*). This band occurs at 340 cm^{-1} in NifEN, just outside the range established for [4Fe-4S]$^{2+}$ clusters with complete cysteinyl ligation [333−339 cm^{-1} (*49*)] and within the range established for clusters with oxygenic ligation at a specific Fe site [339−342 cm^{-1} (*49*, *57*)]. Although this raises the possibility of an oxygenic cluster ligand, the slightly higher (A_1) Fe−S^b frequency could equally well be the result of a hitherto uninvestigated arrangement of coordinating cysteine residues. For example, sequence comparisons with the MoFe protein suggest cluster ligation by three cysteines from the NifE subunit and one from the NifN subunit (see below). This type of subunit bridging arrangement would be unique among Fe−S proteins and hence could account for a slightly higher frequency for the totally symmetric breathing mode.

DISCUSSION

It was previously shown (*31*, *32*) that the products of the FeMo cofactor biosynthetic genes, *nifE* and *nifN*, bear sequence identity when compared to the α- and *β*-subunits of the MoFe protein, respectively. In other words, NifE has a primary sequence similar to NifD (MoFe protein α-subunit), and NifN has a primary sequence similar to NifK (MoFe protein *β*-subunit). Such primary sequence comparisons, the relative migration patterns of NifD, NifK, NifE, and NifN on two-dimensional electrophoretic gels (*58*), the in vivo mutual stability requirements for NifE and NifN (*58*), and the observation that FeMo cofactor biosynthesis is completed prior to its insertion into the apo-MoFe protein (*30*) led to the hypothesis that NifE and NifN form a complex (*58*) that is structurally homologous to the MoFe protein and which provides a scaffold for one or more steps in FeMo cofactor biosynthesis (*32*). This hypothesis was supported by Paustian et al. (*16*), who purified a tetrameric form of NifEN from *A. vinelandii* and reported evidence showing that the as-isolated NifEN complex contains an Fe−S cluster. In the case of the MoFe protein, there are two different types of metalloclusters, the P cluster and the FeMo cofactor (*1*−*3*). Thus, by analogy to the MoFe protein, it is reasonable to expect that the NifEN complex could also have two types of metalloclusters. One such site within the NifEN complex could be analogous to the MoFe protein P cluster site, while the other provides an FeMo cofactor intermediate assembly site. In this model, the NifEN complex is expected to cycle between a "charged" form that contains an FeMo cofactor

intermediate and a "discharged" form that has released the FeMo cofactor intermediate during maturation of the apo-MoFe protein (*59*). Evidence strongly supporting this possibility was reported by Roll et al. (*18*), who found that the native electrophoretic mobility of the NifEN complex is different in crude extracts prepared from different genetic backgrounds. For example, the native electrophoretic mobility of the NifEN complex present in a NifB-deficient crude extract is different from the native electrophoretic mobility of the NifEN complex present in a crude extract prepared from a strain without *nifHDK*. Importantly, the addition of the B cofactor to a NifB-deficient crude extract alters the native electrophoretic mobility of the NifEN complex so that it assumes the same native electrophoretic mobility as NifEN complex produced from the *nifHDK* deletion strain. Because the originally purified NifEN complex was obtained from a NifB-deficient background, and therefore cannot contain the B cofactor, the question arises about the nature and function of the Fe−S cluster contained in the as-isolated NifEN complex. It should be noted that, although it appears that the B cofactor is attached to the NifEN complex in the early stages of its purification from a NifHDK-deficient background, the NifEN complexes isolated from either a NifB-deficient or a NifHDK-deficient background appear to be identical (*16*). In other words, the B cofactor is lost from the NifEN complex during its purification from a MoFe protein-deficient background. In this regard, we note that our Fe analyses of the isolated NifEN complex reveal that there is more Fe than is needed to accommodate two [4Fe-4S] clusters. Thus, it is possible that the as-isolated NifEN complex does have a small amount of the B cofactor, or B cofactor remnant, bound to it.

To purify enough NifEN complex for rigorous biophysical analyses, gene fusion and affinity purification methods were used to raise the in vivo level of NifEN complex and to facilitate its rapid and efficient purification, respectively. The NifEN complex produced and purified in this way is apparently unaltered in either its in vivo or in vitro activities. In this study, a combination of UV−visible, EPR, VTMCD, and resonance Raman spectroscopies have been used to show that the Fe contained in the as-isolated NifEN complex is organized into two identical $[4Fe\text{-}4S]^{2+}$ clusters. These clusters are ligated to the protein complex for the most part or entirely by cysteine residues, have predominantly $S = {}^1/_2$ ground state in the reduced form, and exhibit a midpoint potential of −350 mV. What then is the function of the [4Fe-4S] clusters contained within the as-isolated NifEN complex? Among the obvious possibilities are the following: (i) they play a structural role in formation or stabilization of the tetrameric complex, (ii) they have a redox function that is necessary for FeMo cofactor formation, (iii) they are FeMo cofactor precursors, or (iv) there is some combination of these possibilities.

Muchmore et al. (*22*) have previously developed a homology model for the three-dimensional structure of the NifEN complex that is based on the crystallographically solved MoFe protein structure (*1*). This model places four cysteine residues (three from NifE, residues 37, 62, and 124, and one from NifN, residue-44) in the geometry appropriate for forming a [4Fe-4S] cluster that is located at the NifE−NifN interface at a position analogous to the MoFe protein P cluster site (Figure 10). We favor this model because the four proposed [4Fe-4S] cysteine ligands, and the proposed FeMo cofactor assembly site cysteine [residue 250 (*31*, *32*)], are the only conserved cysteines among all known NifE and NifN primary sequences (*60*). This model indicates that the NifEN complex [4Fe-4S] clusters are most likely to play structural or redox roles rather than becoming incorporated into the FeMo cofactor during its assembly because it places the proposed [4Fe-4S] cluster sites at positions that are remote from the proposed FeMo cofactor assembly sites (*22*). Site-directed mutagenesis and gene-replacement experiments similar to those used to alter the functional properties of the P cluster (*61*) should be useful in clarifying the functional role of the [4Fe-4S] clusters contained within the NifEN complex. This approach, and the availability of relatively large amounts of purified NifEN complex should also help extend the experimental strategy described Roll et al. (*18*) to clarify the nature of the interaction of the B cofactor with the NifEN complex and to determine if the B cofactor Fe−S core is rearranged or further processed upon its binding to the NifEN complex.

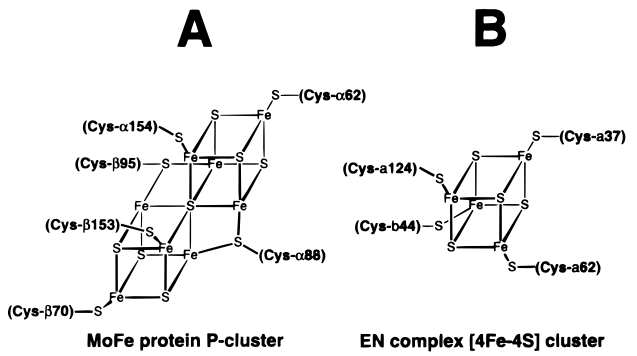

FIGURE 10: Comparison of the structural model for the P cluster (*62*) in its as-isolated P^N state (A) and the proposed structure and organization of the NifEN complex [4Fe-4S] cluster (B). In the scheme for the NifEN complex, residues from the NifE subunit are indicated as a and the residue from the NifN subunit is indicated as b. Primary sequence comparisons (*21*, *33*) indicate that MoFe protein residues α-62, α-88, α-154, and *β*-70 are located at positions equivalent to those of residues a-37, a-62, a-124, and b-44, respectively, in the primary sequence of the NifEN complex.

ACKNOWLEDGMENT

We thank Dr. Vinod Shah for supplying samples of the B cofactor and FeMo cofactor and for providing invaluable advice and Paul Ludden for permitting a portion of this work to be completed in his laboratory. We thank Shannon Garton and Chris Staples for help with the spectroscopic measurements and Amr Ragab for expert technical assistance. We also thank Dr. Jason Christiansen for helpful discussion throughout the preparation of the manuscript.

REFERENCES

1. Howard, J. B., and Rees, D. C. (1994) *Annu. Rev. Biochem. 63*, 235−264.
2. Peters, J. W., Fisher, K., and Dean, D. R. (1995) *Annu. Rev. Microbiol. 49*, 335−366.
3. Burgess, B. K., and Lowe, D. J. (1996) *Chem. Rev. 96*, 2983.
4. Hageman, R. V., and Burris, R. H. (1978) *Proc. Natl. Acad. Sci. U.S.A. 75*, 2699−2702.
5. Hausinger, R. P., and Howard, J. (1983) *J. Biol. Chem. 258*, 13486−13492.
6. Kim, J., and Rees, D. C. (1992) *Nature 360*, 553−560.

7. Lowe, D. J., Fisher, K., and Thorneley, R. N. F. (1993) *Biochem. J. 292*, 93−98.
8. Peters, J. W., Fisher, K., Newton, W. E., and Dean, D. R. (1995) *J. Biol. Chem. 270*, 27007−27013.
9. Lanzilotta, W. N., and Seefeldt, L. C. (1996) *Biochemistry 35*, 16770−17776.
10. Shah, V. K., and Brill, W. J. (1977) *Proc. Natl. Acad. Sci. U.S.A. 74*, 3249−3253.
11. Hawkes, T. R., McLean, P. A., and Smith, B. E. (1984) *Biochem. J. 217*, 317−321.
12. Scott, D. J., May, H. D., Newton, W. E., Brigle, K. E., and Dean, D. R. (1990) *Nature 343*, 188−189.
13. Kim, J., and Rees, D. C. (1992) *Science 257*, 1677−1682.
14. Ludden, P. W., Shah, V. K., Roberts, G. P., Ruttiman-Johnson, C., Rangaraj, P., Foulger, T., Allen, R. M., Homer, M., Roll, J. T., Zhang, X., and Chatterjee, R. (1998) in *Biological Nitrogen Fixation for the 21st Century* (Elmerich, C., Kondorosi, A., and Newton, W. E., Eds.) pp 33−38, Kluwer Academic Publishers, Dordrecht, The Netherlands.
15. Shah, V. K., Allen, J. R., Spangler, N. J., and Ludden, P. W. (1994) *J. Biol. Chem. 269*, 1154−1158.
16. Paustian, T. D., Shah, V. K., and Roberts, G. P. (1989) *Proc. Natl. Acad. Sci. U.S.A. 86*, 6082−6086.
17. Allen, R. M., Chatterjee, R., Ludden, P. W., and Shah, V. K. (1995) *J. Biol. Chem. 270*, 26890−26896.
18. Roll, J. T., Shah, V. K., Dean, D. R., and Roberts, G. P. (1995) *J. Biol. Chem. 270*, 4432−4437.
19. Imperial, J., Ugalde, R. A., Shah, V. K., and Brill, W. J. (1984) *J. Bacteriol. 158*, 187−194.
20. Hoover, T. R., Imperial, J., Ludden, P. W., and Shah, V. K. (1989) *Biochemistry 28*, 2768−2771.
21. Zheng, L., White, R. H., and Dean, D. R. (1997) *J. Bacteriol. 179*, 5963−5966.
22. Muchmore, S. W., Jack, R. F., and Dean, D. R. (1996) in *Mechanisms of Metallocenter Assembly* (Hausinger, R. P., Eichhorn, G. L., and Marzilli, L. G., Eds.) pp 111−132, VCH Publishers, Inc., New York.
23. Gavini, N., and Burgess, B. K. (1992) *J. Biol. Chem. 267*, 21179−21186.
24. Rangaraj, P., Shah, V. K., and Ludden, P. W. (1997) *Proc. Natl. Acad. Sci. U.S.A. 94*, 11250−11255.
25. White, T. C., Harris, G. S., and Orme-Johnson, W. H. (1992) *J. Biol. Chem. 267*, 24007−24016.
26. Homer, M. J., Paustian, T. D., Shah, V. K., and Roberts, G. P. (1993) *J. Bacteriol. 175*, 4907−4910.
27. Paustian, T. D., Shah, V. K., and Roberts, G. P. (1990) *Biochemistry 29*, 3515−3522.
28. Homer, M. J., Dean, D. R., and Roberts, G. P. (1995) *J. Biol. Chem. 270*, 24745−24752.
29. Shah, V. K., Imperial, J., Ugalde, R. A., and Ludden, P. W. (1986) *Proc. Natl. Acad. Sci. U.S.A. 83*, 1636−1640.
30. Ugalde, R. A., Imperial, J., Shah, V. K., and Brill, W. J. (1984) *J. Bacteriol. 159*, 888−893.
31. Dean, D. R., and Brigle, K. E. (1985) *Proc. Natl. Acad. Sci. U.S.A. 82*, 5720−5723.
32. Brigle, K. E., Weiss, M. C., Newton, W. E., and Dean, D. R. (1987) *J. Bacteriol. 169*, 1547−1553.
33. Page, W. J., and von Tigerstrom, M. (1979) *J. Bacteriol. 139*, 1058−1061.
34. Vieira, J., and Messing, J. (1982) *Gene 19*, 259−268.
35. Tabor, S., and Richardson, C. C. (1985) *Proc. Natl. Acad. Sci. U.S.A. 82*, 1074−1078.
36. Robinson, A. C., Burgess, B. K., and Dean, D. R. (1986) *J. Bacteriol. 166*, 180−186.
37. Strandberg, G. W., and Wilson, P. W. (1968) *Can. J. Microbiol. 14*, 25−31.
38. Scott, D. J., Dean, D. R., and Newton, W. E. (1992) *J. Biol. Chem. 267*, 20002−20010.
39. Shah, V. K., Davis, L. C., and Brill, W. J. (1972) *Biochim. Biophys. Acta 256*, 498−511.
40. Smith, P. K., Krohn, R. L., Hermanson, G. T., Mallia, A. K., Gartner, F. H., Provenzano, M. D., Fujimoto, E. K., Goeke, N. M., Olson, B. J., and Klenk, D. C. (1985) *Methods Enzymol. 226*, 199−232.
41. Fortune, W. B., and Mellon, M. G. (1938) *Ind. Eng. Chem. Anal. Ed. 10*, 61−64.
42. Fu, W., Jack, R. F., Morgan, T. V., Dean, D. R., and Johnson, M. K. (1994) *Biochemistry 33*, 13455−13463.
43. Johnson, M. K. (1988) in *ACS Symposium Series* (Que, L., Ed.) pp 326−342, American Chemical Society, Washington, DC.
44. Thomson, A. J., Cheeseman, M. R., and George, S. J. (1993) *Methods Enzymol. 226*, 199−232.
45. Aasa, R., and Vänngård, T. (1975) *J. Magn. Reson. 19*, 308−315.
46. Drozdzewski, P. M., and Johnson, M. K. (1988) *Appl. Spectrosc. 42*, 1575−1577.
47. Johnson, M. K., Robinson, A. E., and Thomson, A. J. (1982) in *Iron−Sulfur Proteins* (Spiro, T. G., Ed.) pp 367−406, Wiley-Intersceince, New York.
48. Onate, Y. A., Finnegan, M. G., Hales, B. J., and Johnson, M. K. (1993) *Biochim. Biophys. Acta 1164*, 113−123.
49. Conover, R. C., Kowal, A. T., Fu, W., Park, J. B., Aono, S., Adams, M. W. W., and Johnson, M. K. (1990) *J. Biol. Chem. 265*, 8533−8541.
50. Conover, R. C., Park, J. B., Adams, M. W. W., and Johnson, M. K. (1991) *J. Am. Chem. Soc. 113*, 2799−2800.
51. Spiro, T. G., Hare, J., Yachandra, B., Gewirth, A., Johnson, M. K., and Remsen, E. (1982) in *Iron−Sulfur Proteins* (Spiro, T. G., Ed.) pp 407−423, Wiley-Interscience, New York.
52. Spiro, T. G., Czernuszewicz, R. S., and Han, S. (1988) in *Resonance Raman Spectra of Heme and Metalloproteins* (Spiro, T. G., Ed.) pp 523−554, John Wiley & Sons, New York.
53. Duin, E. C., Lafferty, M. E., Crouse, B. R., Allen, R. M., Sanyal, I., Flint, D. H., and Johnson, M. K. (1997) *Biochemistry 36*, 11811−11820.
54. Czernuszewicz, R. S., Macor, K. A., Johnson, M. K., Gewirth, A., and Spiro, T. G. (1987) *J. Am. Chem. Soc. 109*, 7178−7187.
55. Fu, W., Morgan, T. V., Mortenson, L. E., and Johnson, M. K. (1991) *FEBS Lett. 284*, 165−168.
56. Fu, W. G., Morgan, T. V., Mortenson, L. E., and Johnson, M. K. (1991) *FEBS Lett. 284*, 165−168.
57. Kilpatrick, L. K., Kennedy, M. C., Beinert, H., Czernuszewicz, R. S., Qui, D., and Spiro, T. G. (1994) *J. Am. Chem. Soc. 116*, 4053−4061.
58. Roberts, G. P., and Brill, W. J. (1980) *J. Biol. Chem. 144*, 210−216.
59. Dean, D. R., Bolin, J. T., and Zheng, L. (1993) *J. Bacteriol. 175*, 6737−6744.
60. Dean, D. R., and Jacobson, M. R. (1992) in *Biological Nitrogen Fixation* (Stacey, G., Burris, R. H., and Evans, H. J., Eds.) pp 763−834, Chapman & Hall, New York.
61. Dean, D. R., Setterquist, R. A., Brigle, K. E., Scott, D. J., Laird, N. F., and Newton, W. E. (1990) *Mol. Microbiol. 4*, 1505−1512.

BI980435N